Published in final edited form as:
Ocul Surf. 2014 January ; 12(1): 46–58. doi:10.1016/j.jtos.2013.11.001.

Ultra High-Resolution Anterior Segment Optical Coherence Tomography in the Diagnosis and Management of Ocular Surface Squamous Neoplasia

Benjamin J. Thomas, MD[1], **Anat Galor, MD**[2], **Afshan A. Nanji, MD**[1], **Fouad El Sayyad, MD**[1], **Jianhua Wang, MD, PhD**[1], **Sander R. Dubovy, MD**[1,3], **Madhura G. Joag, MD**[1], and **Carol L. Karp, MD**[1]

[1]Bascom Palmer Eye Institute, University of Miami Miller School of Medicine, Miami, Florida, USA.

[2]Miami Veteran Affairs Medical Center, Miami, Florida, USA.

[3]Florida Lions Ocular Pathology Laboratory, Miami, Florida, USA.

Abstract

The development of optical coherence tomography (OCT) technology has helped to usher in a new era of in vivo diagnostic imaging of the eye. The utilization of OCT for imaging of the anterior segment and ocular surface has evolved from time-domain devices to spectral-domain devices with greater penetrance and resolution, providing novel images of anterior segment pathology to assist in diagnosis and management of disease. Ocular surface squamous neoplasia (OSSN) is one such pathology that has proven demonstrable by certain anterior segment OCT machines, specifically the newer devices capable of performing ultra high-resolution OCT (UHR-OCT). Distinctive features of OSSN on high resolution OCT allow for diagnosis and differentiation from other ocular surface pathologies. Subtle findings on these images help to characterize the OSSN lesions beyond what is apparent with the clinical examination, providing guidance for clinical management. The purpose of this review is to examine the published literature on the utilization of UHR-OCT for the diagnosis and management of OSSN, as well as to report novel uses of this technology and potential directions for its future development.

Keywords

anterior segment OCT; Fourier-domain OCT; high-resolution OCT; ocular surface squamous neoplasia; optical coherence tomography (OCT); slit lamp OCT; spectral domain OCT; swept-source OCT; time-domain OCT; ultra high-resolution OCT

Corresponding author: Carol L Karp, MD, 900 NW 17th St Miami, FL 33136. Tel: 305-326-156. ckarp@med.miami.edu.

The authors have no commercial or proprietary interest in any concept or product discussed in this article.

I. INTRODUCTION

The diagnosis of ocular disease was dramatically advanced with the advent of optical coherence tomography (**OCT**) and its ability to provide an in vivo, cross-sectional image of ocular tissue. Initially conceived as a means of imaging the posterior segment, OCT devices were later utilized for the anterior segment; however, effective imaging of anterior segment structures was limited by the lower resolution and penetrance of earlier OCT machines.[1] With the development of spectral domain OCT (**SD-OCT**) devices capable of high-resolution imaging up to 5μm (**HR-OCT**), as well as ultra high-resolution devices providing resolution of less than 5 μm (**UHR-OCT**), the anterior segment could be imaged sufficiently to elucidate structural details in the corneal epithelium, corneal stroma, and conjunctiva.[2–6]

With improved axial resolution and imaging speed, these newer devices were able to characterize anterior segment dystrophies and degenerations,[7] as well as to provide noninvasive imaging with reliable correlation to histopathologic specimens.[8] Ocular surface squamous neoplasia (**OSSN**) —a disease that traditionally relies on biopsy for definitive diagnosis— demonstrated consistent features on ultra high-resolution OCT to allow for diagnosis prior to excision of suspicious lesions.[8] This is especially important given the increasing use of primary medical therapy for OSSN. OCT can potentially provide a noninvasive means of diagnosing and differentiating neoplastic epithelial lesions, particularly in the setting of concomitant ocular surface disease. This is fast becoming a critical element in the management of OSSN, and a number of papers have been published reporting these findings.[8–10] The purpose of this review is to examine the data concerning the evolution and utilization of high- and ultra high-resolution OCT devices, specifically in the diagnosis and differentiation of OSSN, and to report novel uses of this technology from Bascom Palmer Eye Institute.

II. OPTICAL COHERENCE TOMOGRAPHY: DEVELOPMENT OF HIGH- AND ULTRA HIGH-RESOLUTION MACHINES

OCT was first reported as a means of imaging ocular structures in 1991.[11] In brief, the technology utilizes a Michelson interferometer, which creates a reference beam of (usually infrared) light against which to measure multiple other beams of light as they return from the variably reflective tissue layers of the eye.[2] The device collects reflected light from the sample and reference beams, thereby creating an interference pattern. Multiple interference patterns are created over the surface of the structure being imaged: in the original time-domain OCT (**TD-OCT**) machines, these multiple readings are generated as a reference mirror moves in a linear fashion over the eye, creating individual A-scans that denote a specific measure of the depth and reflectivity of the underlying tissue. These A-scans are then combined to form a composite, cross-sectional image (B-scan).[3] The utilization of light beams to evaluate ocular tissue allows a higher-depth resolution than other technologies, resolution being a function of the relatively short wavelength of infrared light and the wide bandwidth of the light sources utilized in OCT machines.[3]

This technology, enabled by increased axial resolution, created images that were significantly more detailed than any prior ocular imaging modalities. The posterior segment was the first ocular structure to be imaged, followed by the first reported use of anterior segment OCT in 1994 by Izatt, et al.[1] A number of commercially available TD-OCT machines were subsequently designed for imaging of the anterior segment, and posterior segment OCT machines, such as the Stratus OCT (Carl Zeiss Meditec, Dublin, CA), were utilized as well.[2] The earlier devices were capable of achieving sufficient axial resolution and penetrance (higher with higher wavelength light emission) to image the cornea, anterior chamber, and angle[12,13]; detailed images of the anterior segment were still to come.

These earlier TD-OCT devices were somewhat limited compared to newer technologies. First, the reference mirror was required to physically move as it processed serial A-scans, limiting the number of A-scans from 200 per second to little more than 2,000 per second.[14,15] Lengthier scan times were subject to limitations of patient compliance and vulnerable to motion artifact, and relatively fewer A-scans translated into less detailed images.[2] One of the first commercially available machines, the Zeiss OCT1 (Carl Zeiss Meditec, Dublin, CA), yielded an axial resolution of 15 μm and could obtain only 100 A-scans per second.[16] The next model, the Zeiss OCT2 (Carl Zeiss Meditec, Dublin, CA), was capable of being used in a single study to measure tear meniscus height.[17] The later Stratus OCT (Carl Zeiss Meditec, Dublin, CA) machines were capable of an axial resolution of 10 μm and 512 A-scans in 1.3 seconds and yielded only basic images of the anterior segment.[18]

Two commercially available anterior segment OCT (**AS-OCT**) machines were marketed in 2001, both employing time-domain technology: the Slit Lamp OCT (**SL-OCT**) (Heidelberg Engineering, Heidelberg, Germany) and the Visante OCT (Carl Zeiss Meditec, Dublin, CA). Both of these instruments were capable of up to 2,048 A-scans per second,[19] significantly improving image quality, and—by increasing the wavelength of their light source to 1300–1310 nm from the 800 nm source used by such machines as the Stratus OCT—were able to improve their penetrance to a depth of approximately 6–7 mm while reducing signal scattering, sufficient to comprehensively image the structures of the anterior segment.[18] Both machines further improved on the baseline TD-OCT format by allowing for a 15–16 mm scan width that could encompass all anterior segment structures in question, with options to reduce scan width and augment resolution of particular structures.[3]

Still, image resolution for the Visante OCT and SL-OCT was limited to 18 μm and 25 μm, respectively.[18,20] Not until the transition from TD-OCT devices to SD-OCT devices using a broadband light source were significant improvements in image resolution achieved.[2] These newer devices, also known as Fourier-domain OCT (**FD-OCT**), dramatically enhanced the quality of their images by replacing the mobile reference mirror of TD-OCT devices with systems that rely on a spectrometer and high-speed camera to simultaneously capture and decode the multiple spectra containing the depth information across the whole scan.[18] This information is then translated into depth images using the mathematical calculations elucidated by French mathematician Joseph Fourier: each individual point of light reflection generates a localizing return signal of particular intensity, or an “interferometric fringe.” This intensity profile of the source spectrum is then translated into a measurement of frequency, which is proportional to its distance from the light source (ie, its axial location), and the composite signals generate the overall image. This translation is done using Fourier’s equations for the decomposition of a periodic function into a sum of simple sinusoidal-based oscillating functions, known as *Fourier transforms*.[19] Hence, the title of “Fourier-domain” is given to these technologies. Again, the source A-scans are all captured simultaneously, resulting in increased speed of image acquisition.[3]

Freed from the mechanical limitations of a moving reference mirror, these newer devices were capable of compiling as many as 53,000 A-scans per second,[19] significantly increasing signal-to-noise ratio and creating much more detailed images of ocular structures. This advancement was, in most commercially available devices, combined with movement tracking software to help minimize motion artifact.[19] In addition to the improved speed, the use of the OCT light sources with broad bandwidths further improved the axial resolution, providing enhanced details of the tissue structure.[3]

These technologies were initially designed for posterior segment imaging. Adapted lenses and/or software were then designed to enable imaging of the anterior segment. The Cirrus device (Carl Zeiss Meditec, Dublin, CA), Spectralis (Heidelberg Engineering, Heidelberg,

Germany), a handheld Bioptigen model (Bioptigen Inc., Research Triangle Park, NC), and 3D–OCT (Topcon Medical Systems, Oakland, NJ), as well as others,[21–24] are examples of SD-OCT used for imaging of the anterior segment. These devices were capable of axial resolutions from 4–7 μm[19,21] and allowed imaging of sufficient detail to distinguish the epithelium from the stroma, demonstrate epithelial ingrowth at a flap interface after laser in situ keratomilieusis (**LASIK**), and even demonstrate residual foreign bodies not apparent on clinical examination.[22]

However, these newer devices did have one distinct disadvantage compared to the TD-OCT devices such as the Visante and SL-OCT: their horizontal scan width was limited to 3–6 mm, making comprehensive scanning of wider structures —such as simultaneous scanning of the upper and lower tear menisci— difficult, if not impossible.[2] Even the RTVue-100 and iVue-100 devices (Optovue Inc., Fremont, CA), developed in 2007 and 2009 as dedicated AS-OCT machines, were limited to a 6 mm horizontal scan width.[22] Thus, SD-OCT devices were able to generate markedly improved images of anterior segment structures due to their higher resolution, but were limited in certain cases by their scan width and depth. Only swept-source OCT **(SS-OCT)** — a slightly different form of FD-OCT, found in such devices as the SS-1000 CASIA (Tomey, Nagoya, Japan) which utilizes a light source with a 1310 nm wavelength and a 16 mm horizontal scan width-- equaled the scan width of TD-OCT devices, but carried an axial resolution of only 10 μm.[22] These newer SD-OCT machines represented a marked advancement in image quality and diagnostic ability, but were still only a step along the way toward the ideal AS-OCT.

Only with the advent of OCT machines capable of producing ultra high-resolution images of 1–4 μm was it possible to image the detailed components of the cornea.[2] The first report of UHR-OCT was of the imaging of Bowman's layer by a TD-OCT machine capable of 2–3 μm resolution by Drexler et al in 2001.[25] Corneal OCT imaging in vitro of 1 μm axial resolution was reported in 2004,[26] although most subsequent devices were capable of axial resolution of 2–4 μm, with scan widths of 5–12 mm.[27–31] This higher resolution was achieved by using a light source with a broad bandwidth of more than 100 nm, as well as a specifically designed spectrometer that detected the fringes collected from both reference and sample arms.[2] Clinically, this allowed for the detailed imaging of the tear film,[28,30] tear meniscus,[28] contact lens[28–33] interfaces, and individual corneal layers.[31,33–36] Two commercially-available UHR-OCT devices also exist —the Bioptigen SD-OCT (Bioptigen Inc., Research Triangle Park, NC) and the Copernicus HR SOCT (Optopol Technologies SA, Zawiercie, Poland), with axial resolutions of about 3 μm. However, much published data regarding UHR-OCT are based upon the images from custom-built machines.[27–36]

Our institution has constructed a custom-built UHR-OCT machine capable of both high-and ultra high-resolution imaging, with an axial resolution of approximately 2–3 μm in tissue (Figure 1)[2,8] This device uses a 3-module super-luminescent diode light source (Broadlighter, T840-HP, Superlumdiodes Ltd., Moscow, Russia) with a center wavelength of 840 nm —similar in wavelength to other SD-OCT machines, but with a much broader bandwidth light source.[2,7–10] This low-coherence light is passed through a pigtailed isolator, then coupled into a fiber-based Michelson interferometer (see above), and generates up to 24,000 A-scans per second.[2,7–10]

Based on our experience with this device, certain scan parameters can be recommended: a raster scan with 512 (A-scan) × 2014 (depth) × 128 (frame) pixels with a field of view 8 × 8 mm^2 is recommended. This will allow for coverage of the lesion to the estimated lesion margin in most cases. If the scan area is not big enough, the scan dimension should be increased up to 10 × 10 mm^2. Usually, multiple scans will be needed with horizontally and vertically oriented scans. For the generated two-dimensional scan images, a scan of 2048

(A-scan) × 2048 (depth) pixels provides high-definition cross-sectional images of sufficient size. Often scanning the junction of normal and abnormal tissue is most helpful for diagnosis.

With routine use of this device at our institution, we have been able to image both normal and diseased anterior segment structures with remarkable detail, allowing increased understanding of a number of anterior segment diseases, including OSSN.

III. UHR-OCT FOR DIAGNOSIS OF OSSN

The classic presentation of OSSN has been well described.[37–41] Elevated, papillary, gelatinous, or leukoplakic lesions are easily suspected as OSSN, especially when corroborated by rose bengal staining or epidemiologic risk factors in a particular patient.[38,40] However, sometimes the clinical diagnosis is not so evident. Given the breadth of the differential diagnosis of OSSN, which includes pterygium, pingueculum, actinic disease, dyskeratosis, amelanotic melanoma, papilloma, nevi, scar tissue, anterior basement membrane dystrophy, pseudoepitheliomatous hyperplasia, and corneal pannus,[9,42] differentiation of OSSN, especially in the setting of concomitant ocular surface disease, may be challenging.

The diagnosis of OSSN classically relies on histological examination of tissue specimens, and excisional biopsy remains the gold standard for diagnosis and treatment.[8,40] However, as medical treatment is now frequently utilized for OSSN, noninvasive methods for diagnosis are becoming increasingly important.[8–10,42] These modalities include high-resolution anterior segment ultrasound biomicroscopy (**UBM**),[43] in vivo confocal microscopy,[44] and OCT.[8–10] Each imaging modality has the advantage of being noninvasive, and each has been shown to be useful in the detection of OSSN.[8,43,44] However, both UBM and some confocal microscopy devices require contact with the ocular surface,[8,45], increasing both the length of time and technical expertise required for their performance. Furthermore, although confocal microscopy has the advantage of detailing individual cell morphology, something currently outside of the capability of UHR-OCT, it images a very limited area.[8,44,46] Both OCT and UBM provide a broader morphological view of a lesion and show good correlation with tissue measurements. OCT has the advantage of higher-resolution images, but shadowing may occur in thick lesions or those with leukoplakia.[45] UBM has greater depth of penetrance but lower resolution.

With the development of high (5–10 μm) and ultra high (<5 μm) resolution-OCT devices, resolution of the epithelium from underlying tissue layers[21,47] was possible, and the door was opened to more precise diagnosis of OSSN by noninvasive diagnostic methods. In the first series looking at UHR-OCT and OSSN published by Abou Shousha et al in 2011, images of OSSN lesions of seven patients obtained by UHR-OCT were compared to their subsequent histological appearance.[8] Significant correlation was noted, and the authors concluded that three features on UHR-OCT were considered classic for a diagnosis of OSSN: 1) a thickened hyper-reflective epithelial layer, 2) an abrupt transition from normal to abnormal epithelium, and 3) a distinct plane between the lesion and underlying tissue that could be noted in conjunctival intraepithelial neoplasia (seen in thinner tumors).[8] These abnormal features were noted to normalize with successful medical therapy, as seen in Figure 2 and, later, in Figure 9.[8,10] Additional studies have demonstrated the ability of UHR-OCT to image other anterior segment neoplasias, such as lymphoid and pigmented lesions,[5,48–50] although full discussion of these findings is beyond the scope of this article.

IV. OCT FOR EXCLUSION OF OSSN

With the OCT characteristics of OSSN established, attention is now turning to the potential of OCT to differentiate OSSN from other dystrophic, degenerative, and neoplastic changes of the ocular surface. One of the first studies, published in 2011 by Vajzovic et al, described a series of 59 patients, with reported findings of UHR-OCT imaging of anterior segment dystrophies and degenerations, including some with OSSN.[7] The custom-built UHR-OCT machine was able to generate images of sufficient quality to demonstrate various deposits within particular layers of the cornea, creating highly specific images for such diseases as Salzmann's nodular degeneration and demonstrating the previously listed classic features of OSSN.[7] In their discussion, the authors raised the question of the role of UHR-OCT in managing OSSN, including the possibility of detecting early subclinical recurrences of neoplastic disease, although this had not yet been observed.

The series by Vajzovic et al raised an equally important question: if UHR-OCT is able to generate distinctive images of both OSSN and other, non-neoplastic lesions, could it be utilized to distinguish OSSN from other anterior segment diseases? Kieval et al reported the UHR-OCT findings in a series of 34 patients with either OSSN or pterygia, a degenerative pathology that can sometimes be confused with OSSN.[9] The authors reported that they could reliably distinguish pterygia from OSSN by UHR-OCT, and that UHR-OCT images consistently correlated with histopathologic specimens from the same eye.[9] UHR-OCT images of pterygia demonstrated a thin, dark layer of epithelium with the presence of a subepithelial hyper-reflective tissue (Figure 3), while OSSN showed the previously cited features of thickened and hyper-reflective epithelium, with distinct transition zones (Figure 2). Differences in epithelial thickness between the two entities were statistically significant, to such a degree that a cutoff value of 142 μm for epithelial thickness was able to reliably differentiate pterygia from OSSN with a sensitivity of 94% and a specificity of 100%.[9] Further, the authors noted that 12 of the 17 OSSN lesions were identifiable by clinical examination alone, but that the remaining 5 (mostly corneal lesions) were subtler in presentation, and UHR-OCT was critical in allowing differentiation of these lesions.[9]

Additionally, in papers by both Vajzovic et al[7] and Hurmeric et al,[51] UHR-OCT was used to diagnose an atypical presentation of Salzmann's nodular degeneration that was initially diagnosed as OSSN. In these reports, the UHR-OCT of the Salzmann's nodules revealed thin, normal epithelium and a subepithelial lesion. Other than these reports, no further published data exist regarding the potential of UHR-OCT to differentiate masquerading anterior segment lesions from OSSN.

Thus, a significant knowledge gap exists in the potential role of UHR-OCT in the differentiation of OSSN in the setting of complex ocular pathology: beyond pterygia and Salzmann's nodular degeneration, is UHR-OCT capable of distinguishing OSSN from other degenerative and dystrophic lesions? This question is critical for any ophthalmologist confronted with a potentially neoplastic lesion, especially in the setting of a chronically disturbed ocular surface, as is often the case at our tertiary eye care institute. Regular use of UHR-OCT in suspected cases of OSSN, often referred from outside ophthalmologists, has generated a number of cases wherein OSSN was initially suspected but UHR-OCT was able to suggest an alternate diagnosis.

Figure 4 demonstrates the clinical examination of a 77-year-old male referred to our clinic out of concern for OSSN. The patient presented with a corneal lesion that had a large feeder blood vessel and a papillary appearance (Figure 4A). There had been a recent change in the lesion, suggesting possible neoplasia. An UHR-OCT of the lesion (Figure 4B) showed a uniform, hyporeflective epithelium with an intensely hyper-reflective subepithelial

deposition. Notably absent were the neoplastic stigmata of OSSN, including thickened, hyper-reflective epithelium or a distinct transitional zone. The findings were consistent with a subepithelial lipid deposition, not OSSN.

Figure 5 illustrates critically important use of the UHR-OCT. This patient was referred to our clinic out of concern for an enlarging lesion at the superotemporal corneal limbus, thought to be OSSN (Figure 5A). Numerous "feeder vessels" were noted, and the lesion had a gelatinous appearance similar to OSSN. UHR-OCT, however, demonstrated that the mass was clearly subepithelial, with thin overlying epithelium (Figure 5B), inconsistent with a diagnosis of OSSN. This OCT finding, along with the subjacent conjunctival pigment, raised clinical suspicion of a mostly amelanotic melanoma, and excisional biopsy confirmed this (Figure 5C). Expeditious surgical treatment of the melanoma lesion was thus aided by early use of UHR-OCT, which excluded OSSN as a diagnosis.

Our custom-built UHR-OCT has also been useful in excluding OSSN in cases of nodular scleritis, inflamed pingueculae, and atypical-appearing pterygia, when the clinical diagnosis was not clear.

These cases illustrate the potential of UHR-OCT technology to supplement clinical impressions and perform ocular surface surveillance in the setting of complex ocular surface disease. Ideally, these devices will help the clinician avoid unnecessary corneal and conjunctival scarring or limbal stem cell deficiency from multiple biopsies or surgical excisions.[52,53]

V. OCT FOR DETECTION OF OSSN IN THE SETTING OF CONCOMITANT OCULAR SURFACE DISEASE

Similar to its function in ruling out OSSN, a potential role of the UHR-OCT is to detect OSSN in the setting of concomitant ocular surface disease. Previous reports have largely focused on atypical presentations of non-neoplastic disease[51] or subtle presentations of OSSN[9]; however, there are no reports highlighting cases wherein OCT was employed to detect OSSN in the setting of complex anterior segment scarring or degeneration.

OSSN is known to masquerade as scar tissue or pannus[40,42,54]; additionally, it can appear in association with pterygia and has been associated with chronic ocular surface inflammation, atopic ocular surface disease, and chemical injury.[54–57] Each pathology can potentially obscure the diagnosis of OSSN. Thus, the question of using UHR-OCT for the detection of OSSN in the setting of concomitant ocular surface disease is an important one.

UHR-OCT can also be used to monitor patients for OSSN and other ocular surface neoplasia. It can be most helpful in the setting of complex concomitant ocular surface diseases in which a clinical recurrence may be difficult to detect. Figure 6 represents a patient positive for human immunodeficiency virus (**HIV**) with a complex ocular surface, including a history of vernal keratoconjunctivitis and limbal stem cell deficiency (**LSCD**), as well as a history of previously treated OSSN. He was referred for biopsy because of changes in the appearance of his limbal conjunctiva. The patient's baseline ocular surface was a vascularized cornea with fragile epithelium from his LSCD. However, at presentation, raised reddish, "fleshy" changes were noted at the limbus from 2–4 o'clock and 8–10 o'clock, along with some increased opacification/opalescence on the cornea nasally (Figure 6A). The patient's history raised significant suspicion for neoplasia; however, additional biopsies could potentially contribute to worsening of the patient's concurrent LSCD.[52,53]

UHR-OCT was performed, which demonstrated clear epithelial thickening and hyper-reflectivity, consistent with OSSN (Figure 6B). With this knowledge, a decision to biopsy the limbal lesions was made, and subsequent pathology confirmed recurrent OSSN (Figure 6C). The patient then underwent medical therapy with topical interferon alfa-2B drops, and UHR-OCT assumed a different role: the patient was regularly imaged using UHR-OCT to help confirm the resolution, then absence, of OSSN in a chronically disturbed ocular surface (Figure 6D–E). In 2 years of followup, no neoplastic lesions have been observed, and the patient's LSCD has been stable. UHR-OCT, in this case, was able to both diagnose OSSN in the presence of other ocular surface disease and to monitor treatment and resolution.

In another case, a 76-year-old male with a history of Salzmann's nodular degeneration presented with change in appearance of a previously documented nasal nodule, as well as increased haziness of the cornea surrounding the nodule (Figure 7A). UHR-OCT revealed a focus of subepithelial fibrosis consistent with Salzmann's nodular degeneration, but, more importantly, the UHR-OCT was able to detect an area of hyper-reflective epithelium with an abrupt transitional zone, consistent with OSSN (Figure 7B). The patient underwent an excisional biopsy with adjuvant cryotherapy, and the subsequent pathology confirmed Salzmann's nodular degeneration with concurrent OSSN (Figure 7C). Followup examination at 2 years showed no recurrence (Figure 7D), which was confirmed by UHR-OCT (Figure 7E).

Figure 8A demonstrates the clinical presentation of a 27-year-old patient with a history of LSCD and subsequent corneal scarring. He was referred to our clinic for evaluation of his presumed band keratopathy; however, an area of suspicious thickening was noted amidst the corneal scarring (Figure 8A). UHR-OCT images demonstrated thickened, hyperreflective epithelium with underlying scar tissue (Figure 8B). The lesion was biopsied and subsequent pathology from the cornea revealed dysplastic epithelium (Figure 8C). The patient was then treated for OSSN.

UHR-OCT has been able to demonstrate the presence of focal neoplastic disease in cases of pterygia and Salzmann's nodular degeneration, as well as in cases of HSV keratopathy and "atypical" peripheral corneal infiltrates (suspicious for vernal keratoconjunctivitis) when the clinical diagnosis was unclear. In each case, the UHR-OCT was able to detect areas of thickened, hyper-reflective epithelium with abrupt transition zones from normal epithelium to abnormal epithelium. This prompted subsequent biopsy, and histopathologic examination confirmed the diagnosis of OSSN.

VI. OCT AND THE MANAGEMENT OF OSSN

Another important role for the UHR-OCT is in the detection of subclinical foci of OSSN in patients who are either undergoing topical therapy for OSSN, or who have completed a course of topical therapy and are being monitored for recurrence. This question has been raised previously[7] and reports of the use of UHR-OCT to detect subclinical disease have been published.[8,10] Furthermore, with the increasing prevalence of primary topical medical therapy for OSSN, the importance of UHR-OCT will continue to increase in coming years.

Traditional treatment for OSSN was surgical excision. Treating ocular surface tumors with chemotherapeutic or destructive agents —either as primary or adjuvant therapy— was first reported in 1976, and numerous agents have been employed with varying results, including urea, retinoic acid, dinitrochlorobenzene, and cidofovir, in addition to the primary treatments of mitomycin C (**MMC**), 5-fluorouracil (**5-FU**), and interferon (**IFN**) agents.[58] More recently, the chemotherapeutic agents MMC, 5-FU, and IFN-alfa 2B have been used with great success in the treatment of OSSN and other ocular surface tumors.[41,58–62]

In cases treated by surgical excision, recurrence has been associated with advanced stage, tumor size, and inadequate treatment/positive margins.[63,64] The etiology of recurrence in OSSN treated with primary medical therapy is less well understood. One author hypothesized that subclinical foci of OSSN, not detectable upon slit lamp examination (**SLE**), might serve as a nidus for neoplastic disease.[8] As outlined above, UHR-OCT is capable of detecting subclinical OSSN in the setting of seemingly normal SLE[8,10] and can thereby perhaps prevent the premature termination of medical therapy. One article has reported the use of AS-OCT to detect residual disease after surgical excision in a case of corneal intraepithelial neoplasia; this finding allowed for supplemental medical therapy until resolution of disease.[65]

At our institution, UHR-OCT is employed for regular monitoring of the ocular surface of patients diagnosed with, and treated for, OSSN. UHR-OCT imaging often plays a confirmatory role, affirming the lesion resolution seen upon clinical examination. However, in the course of regular UHR-OCT use, we have encountered patients who were noted to have a disparity between clinical and OCT resolution of tumor (ie, patients had a normal SLE but evidence of residual neoplastic disease shown by UHR-OCT, according to the criteria outlined above). Figure 9 demonstrates one such case. This patient initially presented with a characteristic OSSN lesion (Figure 9A), with the diagnosis confirmed by UHR-OCT (Figure 9B), and elected primary medical therapy with IFN alfa-2B. His followup evaluation appeared to demonstrate clinical resolution (Figure 9C); however, concurrent UHR-OCT showed a persistent focus of epithelial thickening and hyper-reflectivity (Figure 9D). Accordingly, medical therapy with IFN alfa-2B was continued until resolution by both clinical examination (Figure 9E) and UHR-OCT (Figure 9F) was observed.

These cases further characterize the course of OSSN in patients receiving medical therapy alone, allowing greater insight into appropriate treatment paradigms for achieving complete elimination of all neoplastic cells. The optimal duration of treatment is not well known, and diverse lengths of treatment with multiple agents have yielded variable recurrence rates.[59,60] Medical treatment is ideally given until the tumor is fully resolved. In different series, treatment has been carried to clinical resolution,[66–68] up to 1 month beyond clinical resolution,[42,68,69] and up to 4 months beyond clinical resolution.[70] Previously, in our experience, a typical treatment course of primary medical therapy with IFN-alfa 2B or 5-FU was continued for 2 months after clinical resolution is noted, to account for subclinical neoplastic foci. However, our early experience in these cases with a latency period between resolution by clinical examination and UHR-OCT demonstrated a median delay between clinical and OCT resolution of about 16 weeks, with the longest delay being around 29 weeks. This suggests that treatment should probably be carried out for perhaps 16 weeks after clinical resolution in centers where UHR-OCT is not available to directly guide length of therapy.

The incidence of these discrepancies between clinical and UHR-OCT resolution of tumor is not known, and further investigation is warranted. Until then, in our experience, a few approximate guidelines exist to help direct the use of UHR-OCT in the treatment of OSSN. We follow patients who are receiving medical therapy every 6–8 weeks, with serial UHR-OCT imaging. This provides adequate time to detect lesion improvement, but is frequent enough to prevent extended unnecessary medication use. After completion of either medical or surgical treatment, followup every 3–4 months is adequate — again, with serial UHR-OCT imaging. Followup can be done at 6–12 month intervals after a year of normal examinations.

When using UHR-OCT to guide medical therapy, disease resolution and treatment cessation correlate with resolution of the stigmata of OSSN on imaging, ie, normalization of epithelial

appearance across all scans.[8,10] Any return of these stigmata on followup imaging raises concern for disease recurrence, and re-initiation of medical therapy or repeat excisional biopsy can be considered.

Further study is also needed to better characterize the latency period between clinical and OCT resolution, as well as its prognostic significance. These findings will underscore the utility of UHR-OCT technology in the management of OSSN.

VII. Conclusions

As the treatment of OSSN trends toward medical therapy, physicians will need reliable noninvasive forms of diagnosing ocular surface tumors. In particular, the need will arise to distinguish complex, subtle, or atypical cases of OSSN. With the advent of anterior segment imaging using high- and ultra high-resolution OCT machines, these tools can address these growing needs.

Biopsy with histopathological examination remains the gold standard for diagnosing OSSN and other ocular surface lesions. As clinicians increasingly use medical therapy for these lesions, UHR-OCT can assist the clinician in noninvasively diagnosing the presence of OSSN and, importantly, alerting the clinician when a lesion is clearly not an OSSN.

In utilizing this technology, OCT images must be evaluated within the proper clinical context and multiple images must be reviewed, with particular attention to the junction between normal and abnormal tissue. Future studies will be needed to evaluate the role of experience in utilizing the technology and to assess whether images are interpreted consistently. Although no data are available regarding inter- and intra-observer variability for the assessment of ocular surface pathology using the HR-OCT, an early study (employing technology with lower resolution) demonstrated a repeatability of epithelial thickness measurements of 2–3 μm.[71]

Our experience demonstrates that in the diagnosis of OSSN, UHR-OCT can be utilized in challenging scenarios and can be helpful in 1) detecting OSSN in eyes with complex ocular surface pathology, 2) ruling out OSSN in eyes with clinically indeterminate lesions, and 3) monitoring disease resolution and detecting residual sub-clinical disease, especially during medical therapy.

Great progress in the capability and utilization of OCT in the diagnosis and treatment of ocular surface disease does not preclude significant room for improvement. It is hoped that future machines will have improved penetrance and scan width, allowing UHR-OCT to be employed for disease beyond the conjunctival and corneal epithelium. Even higher-resolution machines could perhaps allow imaging to the level of individual cells. Currently, UHR-OCT machines are limited largely to academic institutions, but commercially available machines with more user-friendly interfaces will increase their use in the community. Future study should address potential functions, such as calculation of tumor volume or intraoperative use in designating surgical margins. As the utility of these machines is further explored, development will ideally focus on increased availability, image quality, and interface capability.

In conclusion, the imaging modality of UHR-OCT continues to refine our ability to accurately diagnose ocular surface disease and our understanding of the course and treatment of OSSN. Further validation of its utility in challenging cases with subtle or complex ocular surface disease points to expanded use of this technology in the future.

Acknowledgments

The authors thank Dr. Andre Romano for his expertise.

Supported by NIH Center Core Grant P30EY014801, Research to Prevent Blindness Unrestricted Grant, Department of Defense (DOD- Grant#W81XWH-09-1-0675), Florida Lions Eye Bank, Claire and Lee Hager Grant, Jimmy and Gaye Bryan and the Alicia and Ronald Lepke Grant (all institutional grants).

Abbreviations

5-FU	5-Fluorouracil
AS-OCT	Anterior segment optical coherence tomography
FD-OCT	Fourier-domain optical coherence tomography
HIV	Human immunodeficiency virus
HR-OCT	High-resolution optical coherence tomography
IFN	Interferon
LASIK	Laser in situ keratomilieusis
LSCD	Limbal stem cell deficiency
MMC	Mitomycin C
OCT	Optical coherence tomography
OSSN	Ocular surface squamous neoplasia
SD-OCT	Spectral domain optical coherence tomography
SLE	Slit lamp examination
SL-OCT	Slit lamp optical coherence tomography
SS-OCT	Swept-source optical coherence tomography
TD-OCT	Time-domain optical coherence tomography
UBM	Ultrasound biomicroscopy
UHR-OCT	Ultra high-resolution optical coherence tomography

References

1. Izatt JA, Hee MR, Swanson EA, et al. Micrometer-scale resolution imaging of the anterior eye in vivo with optical coherence tomography. Arch Ophthalmol. 1994; 112:1584–1589. [PubMed: 7993214]
2. Wang J, Abou Shousha M, Perez VL, et al. Ultra-high resolution optical coherence tomography for imaging the anterior segment of the eye. Ophthalmic Surg Lasers Imaging. 2011; 42:S15–s27.
3. Ramos JLB, Li Y, Huang D. Clinical and research applications of anterior segment optical coherence tomography—a review. Clin Experiment Ophthalmol. 2009; 37:81–89. [PubMed: 19016809]
4. Grieve K, Paques M, Dubois A, et al. Ocular tissue imaging using ultrahigh-resolution, full-field optical coherence tomography. Invest Ophthalmol Vis Sci. 2004; 45:4126–4131. [PubMed: 15505065]
5. Simpson T, Fonn D. Optical coherence tomography of the anterior segment. Ocul Surf. 2008; 6:117–127. [PubMed: 18781258]
6. Feng Y, Simpson TL. Corneal, limbal, and conjunctival epithelial thickness from optical coherence tomography. Optom Vis Sci. 2008; 85:E880–E883. [PubMed: 18772715]

7. Vajzovic LM, Karp CL, Haft P, et al. Ultra high-resolution anterior segment optical coherence tomography in the evaluation of anterior corneal dystrophies and degenerations. Ophthalmology. 2011; 118:1291–1296. Epub 2011 Mar 21. [PubMed: 21420175]
8. Shousha MA, Karp CL, Perez VL, et al. Diagnosis and management of conjunctival and corneal intraepithelial neoplasia using ultra high-resolution optical coherence tomography. Ophthalmology. 2011; 118:1531–1537. [PubMed: 21507486]
9. Kieval JZ, Karp CL, Abou Shousha M, et al. Ultra-high resolution optical coherence tomography for differentiation of ocular surface squamous neoplasia and pterygia. Ophthalmology. 2012; 119:481–486. [PubMed: 22154538]
10. Shousha MA, Karp CL, Canto AP, et al. Diagnosis of ocular surface lesions using ultra-high-resolution optical coherence tomography. Ophthalmology. 2013; 120:883–91. Epub 2013 Jan 21. [PubMed: 23347984]
11. Huang D, Swanson EA, Lin CP, et al. Optical coherence tomography. Science. 1991; 254:1178–1181. [PubMed: 1957169]
12. Baikoff G, Lutun E, Ferraz C, Wei J. Static and dynamic analysis of the anterior segment with optical coherence tomography. J Cataract Refract Surg. 2004; 30:1843–1850.
13. Radhakrishnan S, Rollins AM, Roth JE, et al. Real-time optical coherence tomography of the anterior segment at 1310 nm. Arch Ophthalmol. 2001; 119:1179–1185.
14. Stanga PE, Bird AC. Optical coherence tomography (OCT): principles of operation, technology, indications in vitreoretinal imaging and interpretation of results. Int Ophthalmol. 2001; 23:191–197. [PubMed: 11944840]
15. Li Y, Tang M, Zhang X, et al. Pachymetric mapping with Fourier-domain optical coherence tomography. J Cataract Refract Surg. 2010; 36:826–831. [PubMed: 20457376]
16. Pierre-Kahn V, Tadayoni R, Haouchine B, et al. Comparison of optical coherence tomography models OCT1 and Stratus OCT for macular retinal thickness measurement. Br J Ophthalmol. 2005; 89:1581–1585. [PubMed: 16299134]
17. Bitton E, Keech A, Simpson T, et al. Variability of the analysis of the tear meniscus height by optical coherence tomography. Optom Vis Sci. 2007; 84:903–908. [PubMed: 17873764]
18. Jancevski M, Foster CS. Anterior segment optical coherence tomography. Semin Ophthalmol. 2010; 25(5–6):317–323. [PubMed: 21091018]
19. Kiernan DF, Mieler WF, Hariprasad SM. Spectral-domain optical coherence tomography: a comparison of modern high-resolution retinal imaging systems. Am J Ophthalmol. 2010; 149:18–31. [PubMed: 20103039]
20. Hurmeric V, Yoo SH, Mutlu FM. Optical coherence tomography in cornea and refractive surgery. Expert Rev Ophthalmol. 2012; 7:241–250.
21. Maeda N. Optical coherence tomography for corneal diseases. Eye Contact Lens. 2010; 36:254–259. [PubMed: 20724851]
22. Leite MT, Rao HL, Zangwill LM, et al. Comparison of the diagnostic accuracies of the Spectralis, Cirrus and RTVue optical coherence tomography devices in glaucoma. Ophthalmology. 2011; 18:1334–1339. Epub 2011 Mar 5. [PubMed: 21377735]
23. Shetty R, Malhotra C, D'Souza S, et al. WaveLight FS200 vs Hansatome LASIK: intraoperative determination of flap characteristics and predictability by hand-held bioptigen spectral domain ophthalmic imaging system. J Refract Surg. 2012; 28(11 Suppl):S815–s820. [PubMed: 23447894]
24. Tourame, B.; Proust, H.; Ridings, B., et al. J Fr Ophthalmol. Vol. 32. French: 2009. [Spectral-domain optical coherence tomography in anterior segment imaging: the 3rd dimension.]; p. 727-l34.
25. Drexler W, Morgner U, Ghanta RK, et al. Ultra high-resolution ophthalmic optical coherence tomography. Nat Med. 2001; 7:502–507. [PubMed: 11283681]
26. Drexler W. Ultra high-resolution optical coherence tomography. J Biomed Opt. 2004; 9:47–74. [PubMed: 14715057]
27. Ruggeri M, Wehbe H, Jiao S, et al. In vivo three-dimensional high-resolution imaging of rodent retina with spectral-domain optical coherence tomography. Invest Ophthalmol Vis Sci. 2007; 48:1808–1814. [PubMed: 17389515]

28. Wang J, Jiao S, Ruggeri M, et al. In situ visualization of tears on contact lens using ultra high-resolution optical coherence tomography. Eye Contact Lens. 2009; 35:44–49.
29. Gonzalez-Meijome JM, Cervino A, Carracedo G, et al. High-resolution spectral domain optical coherence tomography technology for the visualization of contact lens to cornea relationships. Cornea. 2010; 29:1359–1367. [PubMed: 20847664]
30. Chen Q, Wang J, Tao A, et al. Ultra high-resolution measurement by optical coherence tomography of dynamic tear film changes on contact lenses. Invest Ophthalmol Vis Sci. 2010; 51:1988–1993. [PubMed: 19933178]
31. Shousha MA, Perez VL, Wang J, et al. Use of ultra high-resolution optical coherence tomography to detect in vivo characteristics of Descemet's membrane in Fuchs' dystrophy. Ophthalmology. 2010; 117:1220–1227. [PubMed: 20163865]
32. Kaluzny BJ, Fojt W, Szkulmowska A, et al. Spectral optical coherence tomography in video-rate and 3D imaging of contact lens wear. Optom Vis Sci. 2007; 84:1104–1109. [PubMed: 18091301]
33. Kaluzny BJ, Kaluzny JJ, Szkulmowska A, et al. Spectral optical coherence tomography: a new imaging technique in contact lens practice. Ophthalmic Physiol Opt. 2006; 26:127–132. [PubMed: 16460312]
34. Suh LHS, housha MA, Ventura RU, et al. Epithelial ingrowth after Descemet stripping automated endothelial keratoplasty: description of cases and assessment with anterior segment optical coherence tomography. Cornea. 2011; 30:528–534. [PubMed: 21107249]
35. Hurmeric V, Yoo SH, Karp CL, et al. In vivo morphologic characteristics of Salzmann nodular degeneration with ultra high-resolution optical coherence tomography. Am J Ophthalmol. 2011; 151:248–256. [PubMed: 21145534]
36. Hurmeric V, Yoo SH, Fishler J, et al. In vivo structural characteristics of the femtosecond LASIK-induced opaque bubble layers with ultra high-resolution SDOCT. Ophthalmic Surg Lasers Imaging. 2010; 41(suppl):109–l13. [PubMed: 20128580]
37. Erie JC, Campbell RJ, Liesegang TJ. Conjunctival and corneal intraepithelial and invasive neoplasia. Ophthalmology. 1986; 93:176–183. [PubMed: 3951824]
38. Hamam RB, hat P, Foster CS. Conjunctival/corneal intraepithelial neoplasia. Int Ophthalmol Clin. 2009; 49:63–70.
39. Tunc M, Char DH, Crawford B, et al. Intraepithelial and invasive squamous cell carcinoma of the conjunctiva: analysis of 60 cases. Br J Ophthalmol. 1999; 83:98–103. [PubMed: 10209445]
40. Lee GA, Hirst LW. Ocular surface squamous neoplasia. Surv Ophthalmol. 1995; 39:429–450. [PubMed: 7660300]
41. Shields CL, Shields JA. Tumors of the conjunctiva and cornea. Surv Ophthalmol. 2004; 49:3–24. [PubMed: 14711437]
42. Schechter BA, Koreishi AF, Karp CL, Feuer W. Long-term follow-up of conjunctival and corneal intraepithelial neoplasia treated with topical interferon alfa-2b. Ophthalmology. 2008; 115:1291–l6. [PubMed: 18187195]
43. Finger PT, Tran HV, Turbin RE, et al. High-frequency ultrasonographic evaluation of conjunctival intraepithelial neoplasia and squamous cell carcinoma. Arch Ophthalmol. 2003; 121:168–172. [PubMed: 12583781]
44. Xu Y, Zhou Z, Xu Y, et al. The clinical value of in vivo confocal microscopy for diagnosis of ocular surface squamous neoplasia. Eye (Lond). 2012; 26:781–787. [PubMed: 22402703]
45. Dada T, Sihota R, Gadia R, et al. Comparison of anterior segment optical coherence tomography and ultrasound biomicroscopy for assessment of the anterior segment. J Cataract Refract Surg. 2007; 33:837–840. [PubMed: 17466858]
46. Balestrazzi A, Martone G, Pichierri P, et al. Corneal invasion of ocular surface squamous neoplasia after clear corneal phacoemulsification: in vivo confocal microscopy analysis. J Cataract Refract Surg. 2008; 34:1038–1043. [PubMed: 18499017]
47. Hutchings N, Simpson TL, Hyun C, et al. Swelling of the human cornea revealed by high-speed, ultrahigh-resolution optical coherence tomography. Invest Ophthalmol Vis Sci. 2010; 51:4579–4584. [PubMed: 20435597]
48. Oellers P, Karp CL. Management of pigmented conjunctival lesions. Ocul Surf. 2012; 10:251–263. [PubMed: 23084146]

49. Shah SU, Kaliki S, Shields CL, et al. Enhanced depth imaging optical coherence tomography of choroidal nevus in 104 cases. Ophthalmology. 2012; 119:1066–1072. Epub 2012 Jan 31. [PubMed: 22297027]
50. Bianciotto C, Shields CL, Guzman JM, et al. Assessment of anterior segment tumors with ultrasound biomicroscopy versus anterior segment optical coherence tomography in 200 cases. Ophthalmology. 2011; 118:1297–1302. Epub 2011 Mar 5.
51. Hurmeric V, Yoo SH, Galor A, et al. Atypical presentation of Salzmann nodular degeneration diagnosed with ultra-high-resolution optical coherence tomography. Ophthalmic Surg Lasers Imaging. 2011; 42:e122–e125. [PubMed: 22150601]
52. Schwartz GS, Holland EJ. Iatrogenic limbal stem cell deficiency. Cornea. 1998; 17:31–37.
53. Hatch KM, Dana R. The structure and function of the limbal stem cell and the disease states associated with limbal stem cell deficiency. Int Ophthalmol Clin. 2009; 49:43–52. [PubMed: 19125063]
54. Pe'er J. Ocular surface squamous neoplasia. Ophthalmol Clin North Am. 2005; 18:1–13. vii. [PubMed: 15763187]
55. Oellers P, Karp CL, Sheth A, et al. Prevalence, treatment, and outcomes of coexistent ocular surface squamous neoplasia and pterygium. Ophthalmology. 2013; 120:445–450. Epub 2012 Oct 27. [PubMed: 23107578]
56. Artornsombudh P, Sanpavat A, Tinnungwattana U, et al. Prevalence and clinicopathologic findings of conjunctival epithelial neoplasia in pterygia. Ophthalmology. 2013; 120:1337–1340. Epub 2013 Mar 15. [PubMed: 23499063]
57. Waring GO 3rd, Roth AM, Ekins MB. Clinical and pathologic description of 17 cases of corneal intraepithelial neoplasia. Am J Ophthalmol. 1984; 97:547–559. [PubMed: 6720832]
58. Poothullil AM, Colby KA. Topical medical therapies for ocular surface tumors. Sem Ophthalmol. 2006; 21:161–169.
59. Shah SU, Kaliki S, Kim HJ, et al. Topical interferon alfa-2b for management of ocular surface squamous neoplasia in 23 cases: outcomes based on American Joint Committee on Cancer Classification. Arch Ophthalmol. 2012; 130:159–164. [PubMed: 22332208]
60. Sepulveda R, Pe'er J, Midena E, et al. Topical chemotherapy for ocular surface squamous neoplasia: current status. Br J Ophthalmol. 2010; 94:532–535. [PubMed: 19776089]
61. Parrozzani R, Lazzarini D, Alemany-Rubio E, et al. Topical 1% 5-fluorouracil in ocular surface squamous neoplasia: a long-term safety study. Br J Ophthalmol. 2011; 95:355–359. Epub 2010 Aug 7. [PubMed: 20693564]
62. Chen C, Louis D, Dodd T, et al. Mitomycin C as an adjunct in the treatment of localised ocular surface squamous neoplasia. Br J Ophthalmol. 2004; 88:17–18. [PubMed: 14693762]
63. Yousef YA, Finger PT. Squamous carcinoma and dysplasia of the conjunctiva and cornea: an analysis of 101 cases. Ophthalmology. 2012; 119:233–240. [PubMed: 22189448]
64. Galor A, Karp CL, Oellers P Kao AA, et al. Predictors of ocular surface squamous neoplasia recurrence after excisional surgery. Ophthalmology. 2012; 119:1974–81. Epub 2012 Jun 14. [PubMed: 22704832]
65. Chin EK, Cortes DE, Lam A, et al. Anterior segment OCT and confocal microscopy findings in atypical corneal intraepithelial neoplasia. Cornea. 2013; 32:875–879. [PubMed: 23538623]
66. Holcombe DJ, Lee GA. Topical interferon alfa-2b for the treatment of recalcitrant ocular surface squamous neoplasia. Am J Ophthalmol. 2006; 142:568–571. [PubMed: 17011846]
67. Boehm MD, Huang AJ. Treatment of recurrent corneal and conjunctival intraepithelial neoplasia with topical interferon alfa 2b. Ophthalmology. 2004; 111:1755–1761. [PubMed: 15350333]
68. Schechter BA, Schrier A, Nagler RS, et al. Regression of presumed primary conjunctival and corneal intraepithelial neoplasia with topical interferon alpha-2b. Cornea. 2002; 21:6–11. [PubMed: 11805499]
69. Galor A, Karp CL, Chhabra S, et al. Topical interferon alpha 2b eye-drops for treatment of ocular surface squamous neoplasia: a dose comparison study. Br J Ophthalmol. 2010; 94:551–554.
70. Sturges A, Butt AL, Lai JE, et al. Topical interferon or surgical excision for the management of primary ocular surface squamous neoplasia. Ophthalmology. 2008; 115:1297–1302. [PubMed: 18294690]

71. Wang J, Fonn D, Simpson TL, Jones L. Relation between optical coherence tomography and optical pachymetry measurements of corneal swelling induced by hypoxia. Am J Ophthalmol. 2002; 134:93–98. [PubMed: 12095814]

Figure 1.
Photograph of the custom-built UHR-OCT device employed at Bascom Palmer Eye Institute, Miami, FL, USA.

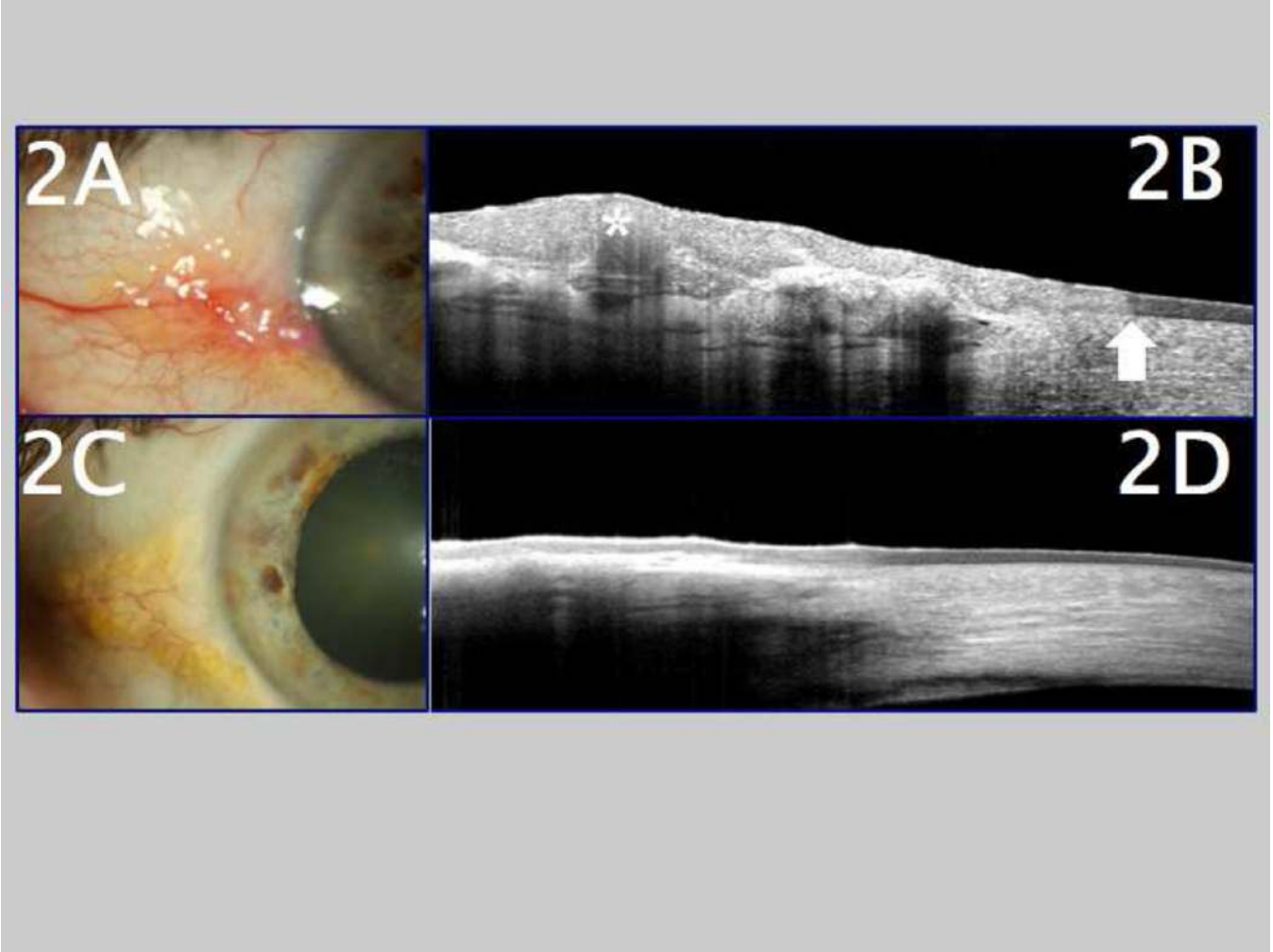

Figure 2.
A. Clinical appearance of ocular surface squamous neoplasia (OSSN) in a patient who presented with an elevated lesion, accompanied by feeder blood vessels, located at the corneoscleral limbus. B. Ultra high-resolution ocular coherence tomography (UHR-OCT) image of the same OSSN lesion, demonstrating a thickened, hyper-reflective epithelium (marked with asterisk) and an abrupt transition zone from normal to abnormal epithelium (arrow). C. Slit lamp photo of the same location after medical therapy for OSSN, showing clinical resolution of the lesion. D. Followup UHR-OCT image of the same eye after medical therapy for OSSN, showing a return of normal-appearing, thin epithelium after resolution of the OSSN.

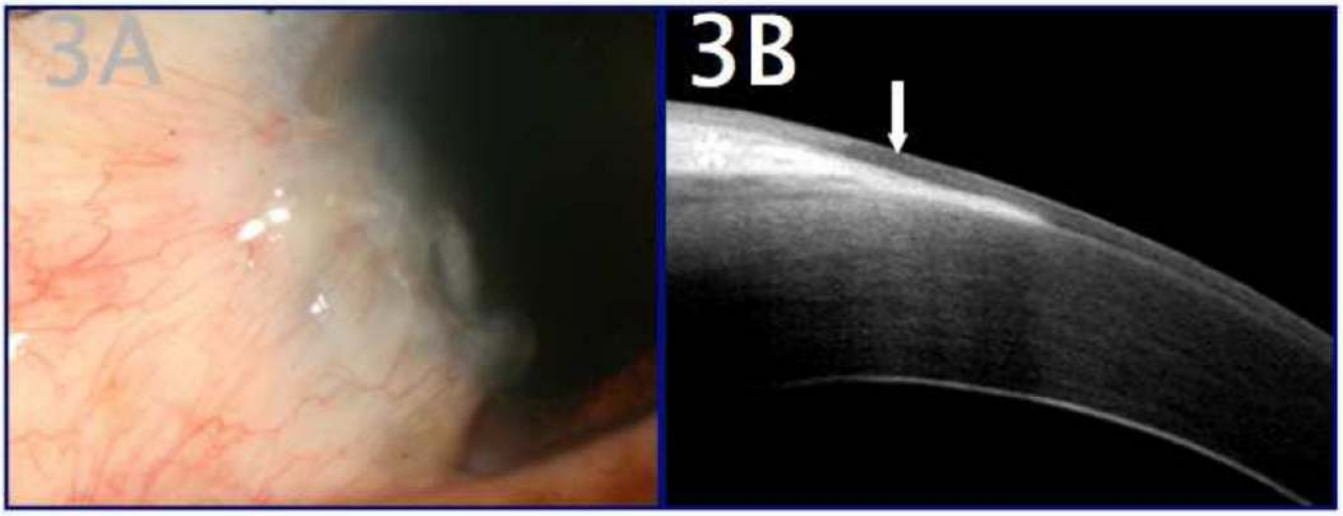

Figure 3.
UHR-OCT image of a pterygium, demonstrating an epithelial layer of normal thickness (arrows) overlying thickened, hyper-reflective subepithelial tissue (marked with asterisk).

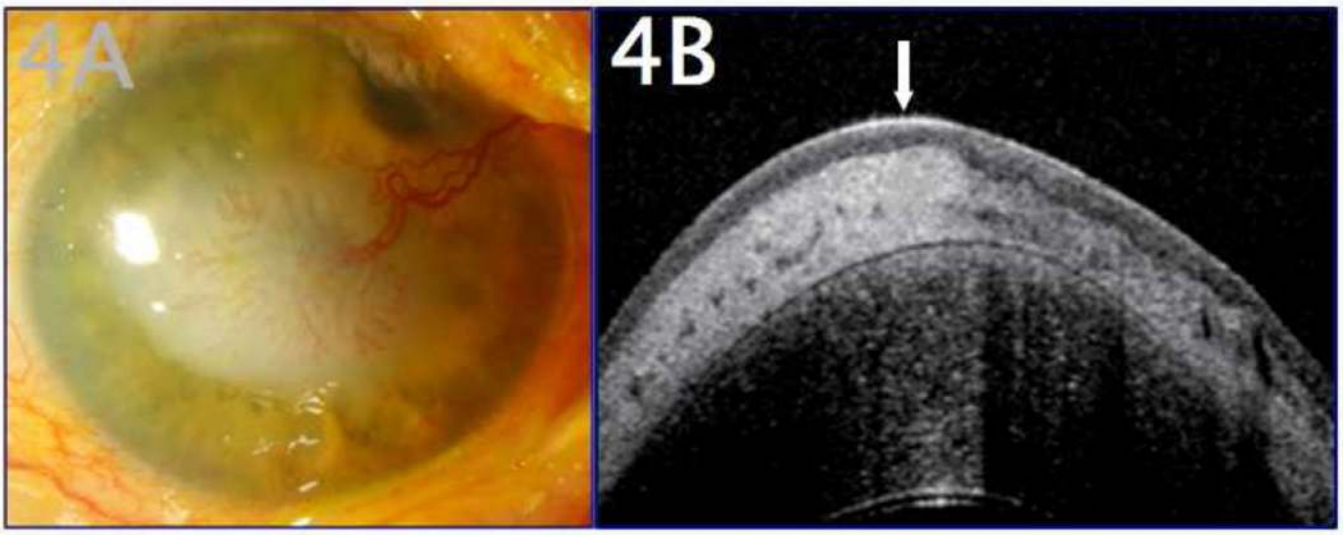

Figure 4.

A 77-year-old male with a history of corneal scarring was referred due to concern for OSSN. A. Clinical examination revealed a white elevated papillary lesion of the cornea with a prominent feeder vessel. B. UHR-OCT revealed a thin, normal hyporeflective epithelium (arrow) and dense subepithelial lesion (marked with asterisk), consistent with subepithelial corneal scarring or lipid. There was no evidence of OSSN by OCT. The patient was followed closely without progressive lesion change and was able to forego excisional procedures of the ocular surface.

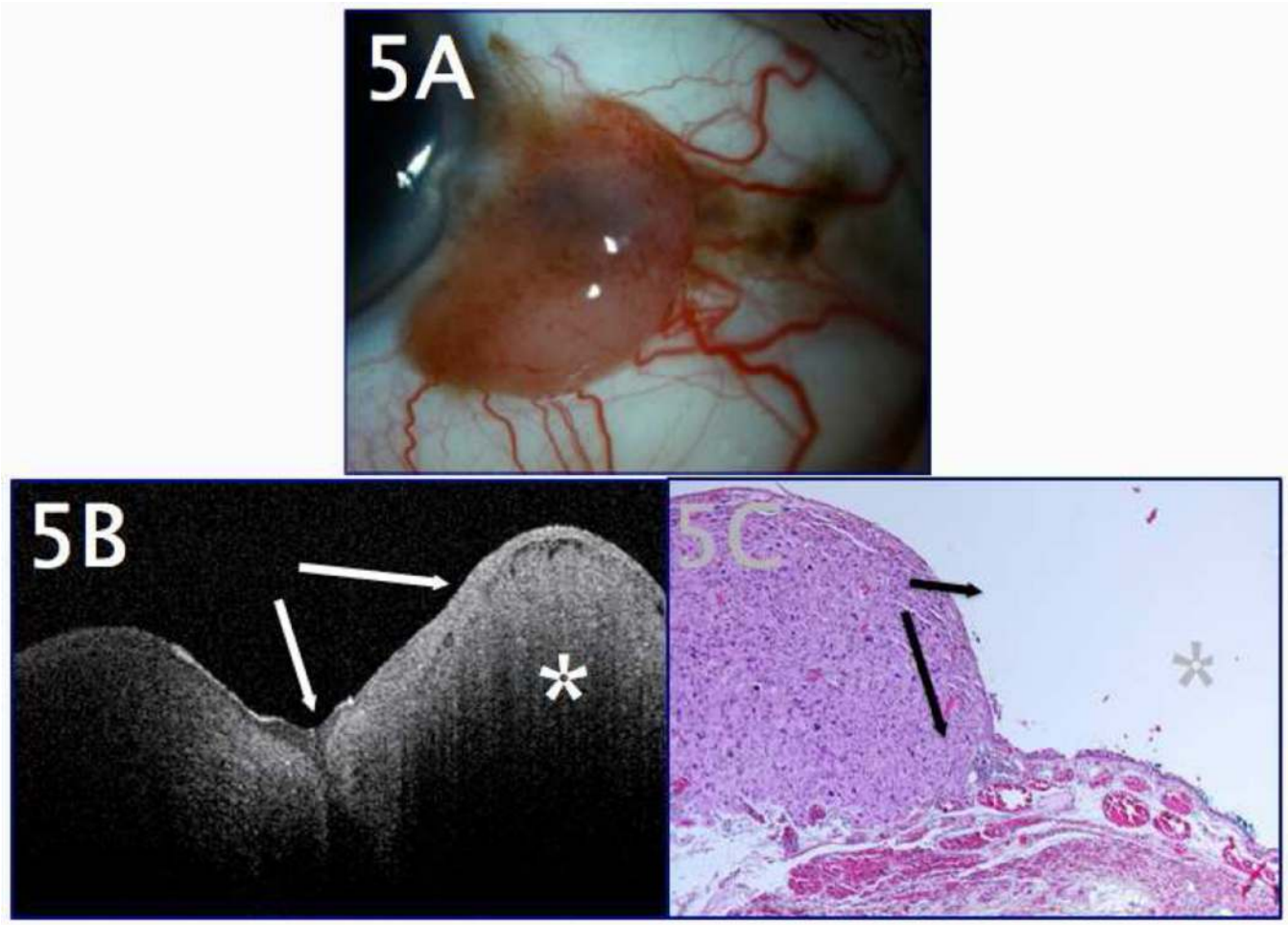

Figure 5.

A 61-year-old male presented for a second opinion regarding a lesion thought to be OSSN. A. Clinical examination revealed a temporal, nodular conjunctival lesion abutting the corneal limbus, which appeared highly vascular with numerous feeder vessels. There were a few adjacent areas of mild pigmentation in the conjunctiva that the patient stated had been present for many years. B. UHR-OCT of the lesion revealed normal-thickness, mildly hyper-reflective epithelium (arrows) overlying a dense subepithelial lesion (marked with asterisk). The finding of a thin epithelium was inconsistent with OSSN. C. Subsequent excisional biopsy (shown in the hematoxylin and eosin (H&E) stain, 20x magnification) revealed non-thickened conjunctival epithelium (arrows) overlying a dense, subepithelial melanocytic lesion (marked with asterisk) that also stained positive for melan A, consistent with melanoma.

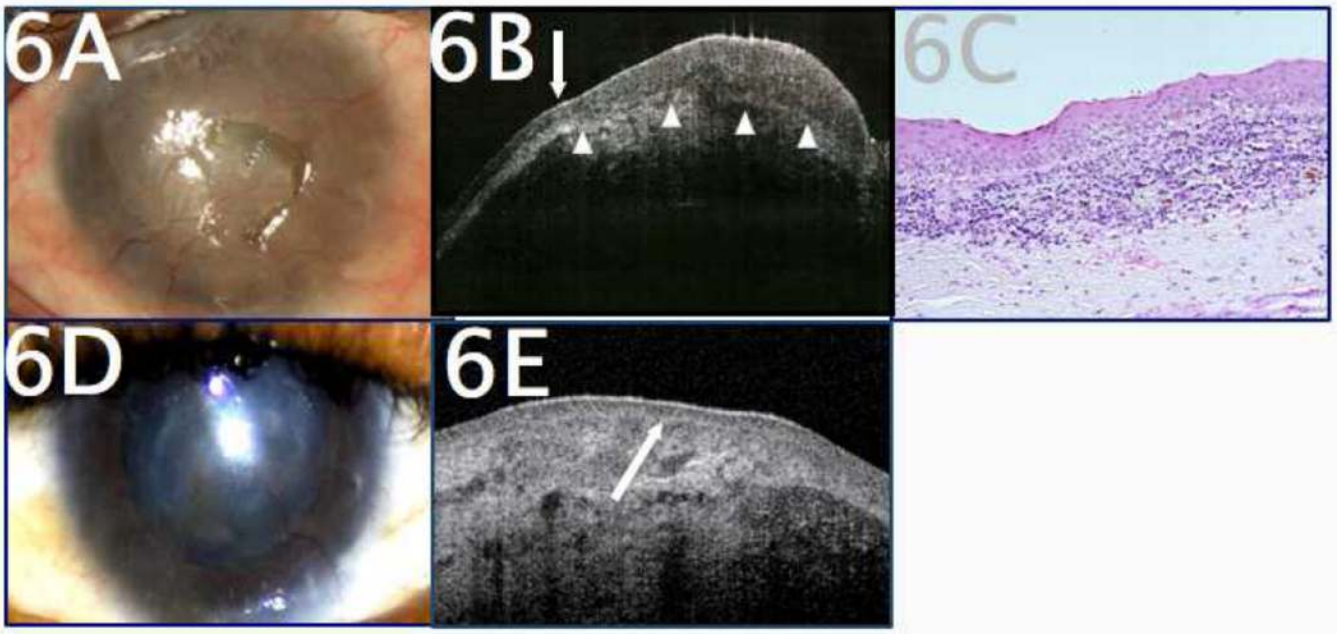

Figure 6.

A 34-year-old HIV-positive male with a history of limbal stem cell deficiency, severe vernal keratoconjunctivitis, and OSSN was referred for changes in corneal and conjunctival appearance, suspicious for OSSN. A. Clinical examination revealed diffuse corneal scarring and neovascularization, making the clinical diagnosis difficult. B. UHR-OCT revealed sudden transition from normal to abnormal epithelium (arrow) as well as a thickened, hyper-reflective epithelium (white arrowheads to mark deep margin of epithelium), findings consistent with OSSN. Subepithelial scarring was also present. C. Histopathology (H&E, 20x magnification) revealed nests of dysplastic epithelial cells with faulty maturation sequences consistent with OSSN. D. After a course of primary medical therapy with interferon (IFN) alfa-2B eyedrops, the areas of disease showed significant improvement, but the patient's baseline ocular surface disease remained, complicating the clinical monitoring of his OSSN to resolution. E. Serial UHR-OCT monitoring demonstrated the return of normal-appearing, non-thickened epithelium (arrow) overlying the patient's corneal scarring, helping to confirm resolution of neoplastic disease.

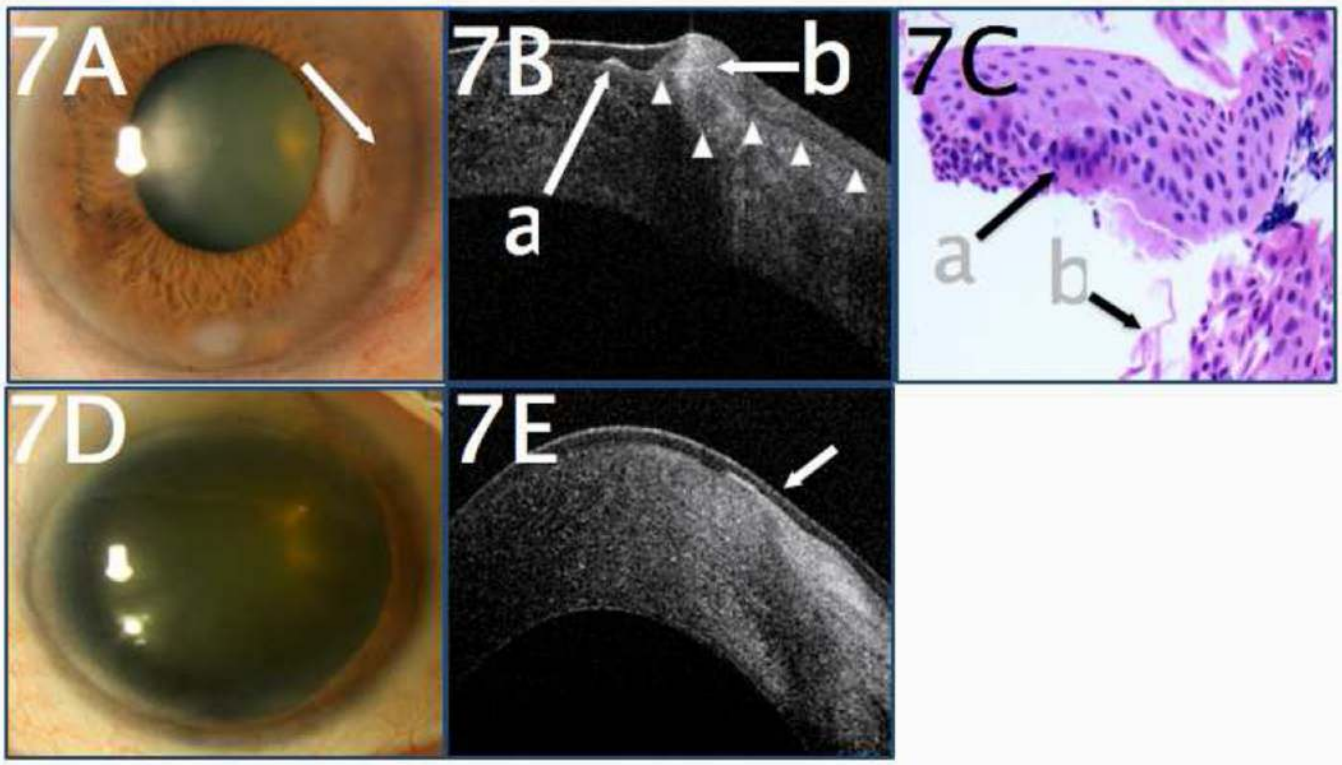

Figure 7.

A. A 76-year-old male with a history of Salzmann's nodular degeneration presented with a change in nodule appearance of a previously-documented nasal nodule with associated corneal haziness (arrow). B. UHR-OCT revealed a focus of subepithelial fibrosis consistent with Salzmann's nodular degeneration (a). Adjacent to this, there was hyper-reflective epithelium (b) with an abrupt transitional from normal to abnormal, consistent with OSSN. White arrowheads indicate the deep margin of the epithelium. C. Histopathologic examination (H&E, 40x magnification) of the epithelial scrapings taken during surgical excision disclosed foci of cellular atypia consistent with OSSN (a), associated with fibrotic material (b). D. Two years after surgical excision, examination showed no evidence of OSSN. E. UHR-OCT two years after excision revealed normal, thin dark epithelium (arrow). There was subepithelial scarring present from the excision and the prior Salzmann's nodule and no evidence of OSSN.

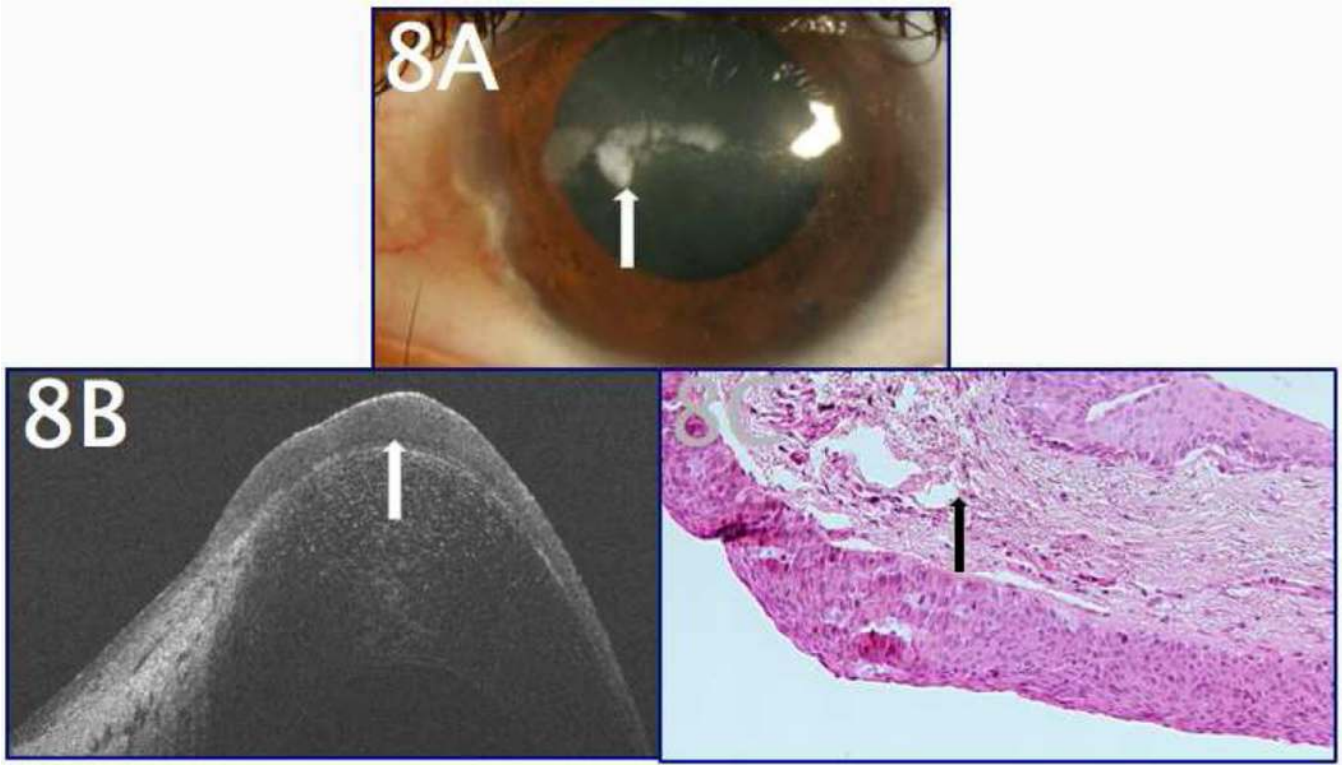

Figure 8.

A 27-year-old male with a history of LSCD and corneal scarring, presumed to be band keratopathy, presented for evaluation of his corneal lesions. A. The appearance was largely consistent with a diagnosis of corneal scarring, but certain areas of the corneal surface appeared slightly elevated (arrow). B. UHR-OCT to evaluate the area of presumed scarring and calcification revealed thickened, hyper-reflective epithelium consistent with OSSN (arrow). C. Subsequent histopathology (H&E, 20x magnification) confirmed the presence of diffusely thickened, dysplastic epithelium with faulty maturation sequences (arrow), consistent with OSSN.

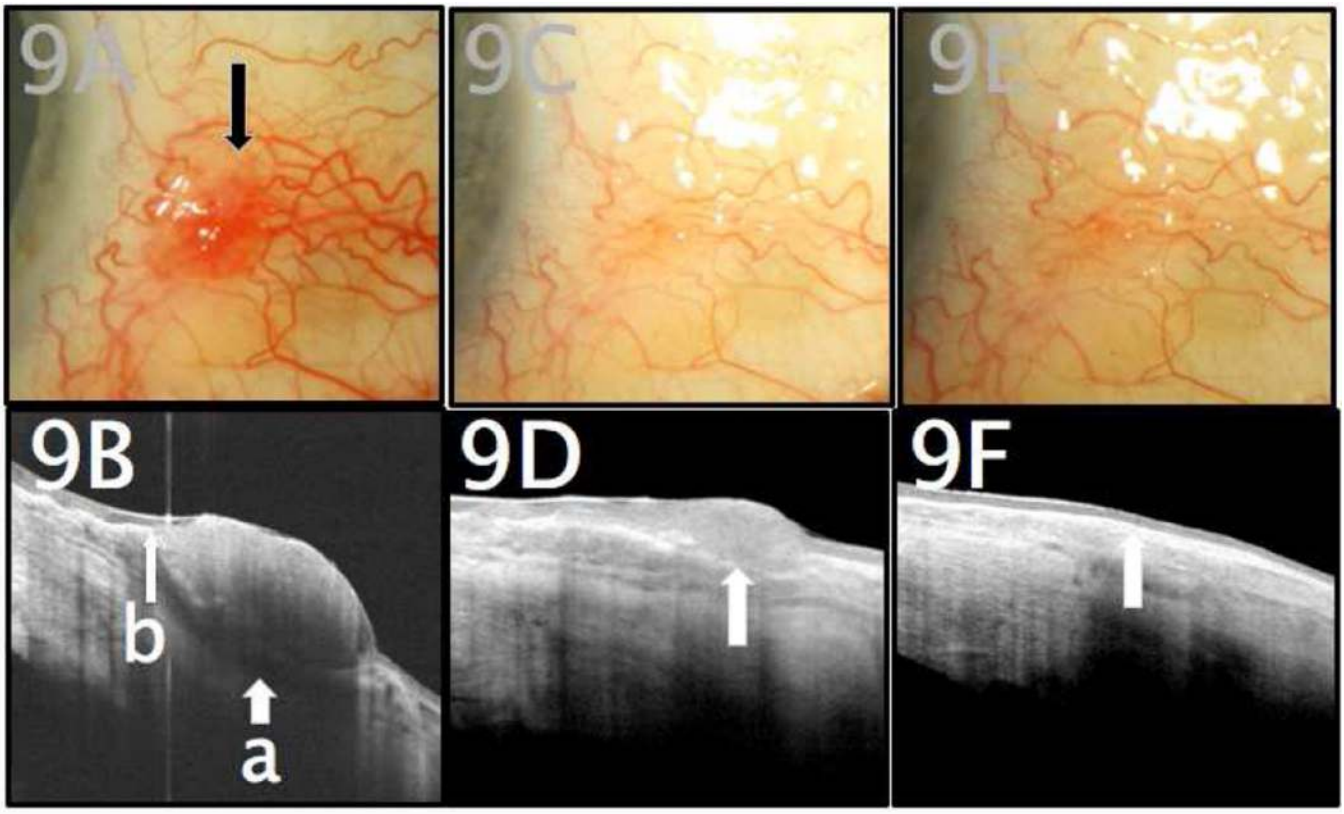

Figure 9.

A. An 83-year-old male with no prior history of ocular surface squamous neoplasia (OSSN) presented with a suspicious conjunctival lesion of the left eye (marked by arrow). B. Initial UHR-OCT imaging revealed a hyper-reflective thickened epithelium (a) and a sudden transition from normal to abnormal tissue (b). C. One month after starting treatment with topical recombinant IFN alfa-2B, the area of previously-affected conjunctiva appeared clinically to be free of tumor. D. UHR-OCT, however, demonstrated a focus of persistently hyper-reflective and thickened conjunctival epithelium (arrow), consistent with OSSN. E. Topical therapy was continued accordingly, and at 3-month follow-up, slit lamp examination continued to demonstrate clinical resolution. F. UHR-OCT confirmed normal epithelial appearance, with resolution of prior hyper-reflectivity and with normalization of epithelial thickness (arrow).

Table 1

Comparison of some anterior segment imaging systems

Instrument	Company	Measurement principle	Axial resolution (Approximate)	Scanning speed (Approximate)	Commercially Available
Stratus OCT	Carl Zeiss Meditec	Time-domain	10 μm	400 A scans per second	Yes
Visante OCT	Carl Zeiss Meditec	Time-domain	18 μm	2000 A scans per second	Yes
Slit-lamp OCT	Heidelberg	Time-domain	25 μm	2,000 A scans per second	Yes
Spectralis OCT	Heidelberg	Spectral-domain	4–7 μm	40,000 A scans per second	Yes
Bioptigen OCT	Bioptigen Inc.	Spectral-domain	5–6 μm	32,000 A scans per second	Yes
Cirrus OCT	Carl Zeiss Meditec	Spectral-domain	5 μm	27,000 A scans per second	Yes
OCT SLO	Optos	Spectral Domain	<6 μm	27,000 A scans per second	Yes
3D OCT 2000	Topcon	Spectral-domain	5 –6 μm	50,000 A scans per second/ 27000 A scans per second	Yes
SOCT Copernicus+	Optopol	Spectral-domain	5 μm	27,000 A scans per second	Yes
RTVue and iVue	Optovue	Spectral-domain	5 μm	26,000 A scans per second	Yes
SS-1000 CASIA	Tomey	Spectral-domain (swept source)	10 μm	30,000 A scans per second	Yes
Ultra high-resolution OCT	Custom-built device	Spectral-domain	~3 μm	24,000 to 26,000 A scans per second (variable)	No

Table 2

Comparison of imaging modalities for the diagnosis of ocular surface squamous neoplasia.

Imaging Modality	Advantages	Disadvantages
Clinical examination	In vivo examination, can assess staining characteristics, mobility of lesion..	Difficult to determine lesion depth precisely, unable to assess cellular morphology.
Biopsy/histopathology	Gold standard: direct examination at cellular level of involved tissues, and the only modality that allows for diagnosis of tissue invasion.	Requires surgical intervention.
Impression cytology	Able to examine superficial tissue at a cellular level.	Only assesses surface cells, not deeper levels.
Ultrasound biomicroscopy (UBM)	High scan penetrance, especially useful for large lesions.	Low resolution, cannot evaluate epithelial versus subepithelial nature of lesion.
Confocal microscopy	Able to examine tissue at a cellular level, directly visualizing cellular atypia,	Limited scan width makes it difficult to get “big picture”, limited depth of evaluation prevents reliable detection of invasion.
Ultra high resolution ocular coherence tomography (UHR-OCT)	High-resolution imaging with cross sectional view; dynamic noncontact scanning modality reduces need for technical expertise compared to confocal microscopy and UBM. Scanning well tolerated by patient.	Poor penetrance with thicker lesions, cannot reliably detect invasion.

Table 3

Comparison of UHR-OCT appearance of various stages of OSSN/other pathologies

Pathology	Diagnostic Features by UHR-OCT	Lesion Image
OSSN	Thickened, hyper-reflective epithelial layer with an abrupt transition from normal to abnormal epithelium. Thicker lesions may exhibit shadowing, obscuring the subepithelial plane.	Figure 2B, 6B, 7B(b), 8B, 9B
OSSN – resolving	Progression toward epithelial normalization: reduced thickness and hyperreflectivity, less distinct transition zone.	Figure 9D
OSSN - resolved	Normalization of epithelial appearance.	Figure 2D, 6E, 7E, 9F
Melanoma/nevi	Normal-thickness or slightly thicker epithelium overlying a subepithelial lesion. The epithelium may have variable hyper-reflectivity. Thick lesions may exhibit significant “shadowing.” NOTE: In nevi, cystic spaces can be seen on UHR-OCT, although this does not exclude malignancy.	Figure 5B
Pterygium	Thin or normal epithelium overlying dense, hyper-reflective, subepithelial lesion. Variable hyper-reflectivity of overlying epithelium.	Figure 3B
Corneal scarring/ Salzmann’s	Normal-thickness epithelium overlying dense, hyper-reflective subepithelial lesion overlying Bowman’s layer.	Figures 4B, 7B(a), 7E

UHR-OCT=Ultra high resolution ocular coherence tomography ; OSSN=ocular surface squamous neoplasia